Mathematical Geology, Vol. 34, No. 4, May 2002 (© 2002)

Integrating Seismic Data for Lithofacies Modeling: A Comparison of Sequential Indicator Simulation Algorithms[1]

Tingting Yao[2]

Clastic reservoir characterization starts typically with modeling lithofacies distribution and geometry. The architecture of the reservoir, governed by the lithofacies geometry, is a major source of heterogeneity in such clastic systems. Seismic data provide potentially valuable information about the areal distribution of different lithofacies, such as the averaged prior proportion of each lithofacies. However, seismic data are available only at coarse vertical resolution rather than the fine lithofacies sampling along wells, hence seismic is considered equivalent to 2D data while building 3D geological models. This scale difference between the seismic data and the lithofacies data available along the wells makes direct integration difficult. Different algorithms have been proposed to integrate the seismic data: (1) duplicate seismic data along the vertical line and use the prior proportions provided by the seismic data as prior local means; (2) integrate the 2D seismic data as collocated block averages; and (3) duplicate seismic data along the vertical line and integrate them using a Markov-Bayes algorithm. These three algorithms are applied on a data set originating from a real clastic reservoir. The results are compared with regard to how much kriging weight is applied to the seismic data and how well the information from seismic data is honored.

KEY WORDS: reservoir, stochastic, facies, modeling, Markov-Bayes model.

INTRODUCTION

The distribution of lithofacies in a clastic reservoir is the most important heterogeneity for reservoir characterization and performance prediction (Haldorsen and Damsleth, 1990). Reservoir modeling of clastic systems starts with modeling lithofacies geometry, followed by the simulation of petrophysical properties within each lithofacies. There are many different approaches to the stochastic modeling of reservoir facies, the two main classes being object-based and cell-based algorithms. Object-based algorithms can generate models displaying the

[1]Received 30 October 2000; accepted 25 June 2001.

[2]ExxonMobil Upstream Research Company, ST 3209, P.O. Box 2189, Houston, Texas 77252; e-mail: tingting.yao@exxon.sprint.com.

crisp geometric shape of the facies, which are consistent with prior geological morphological interpretations (Deutsch and Wang, 1996; Georgsen and Omre, 1993; Omre, Solna, and Tjelmeland, 1990; Stoyan, Kendall, and Mecke, 1987). However, the probabilistic distributions of the shape parameters, required by the object-based algorithms, are difficult to infer from actual subsurface data. In addition, conditioning to dense local data and integrating secondary information can be difficult. In this paper, we will focus on cell-based geostatistical methods for lithofacies modeling.

For cell-based geostatistical methods, the most commonly used is sequential indicator simulation (Journel and Alabert, 1989, 1990). This technique generates lithofacies at each cell of 3D model, one at a time, by drawing from the local conditional cumulative distribution function (ccdf) estimated from the conditioning data. The previously simulated values are to be used as conditioning data for the nodes to be simulated subsequently, hence the spatial structure of the distribution of lithofacies can be reproduced. Compared with objected-based algorithms, sequential indicator simulation can not reproduce the crisp geometric shapes of facies such as channels, since it is based on the two-point statistics of the variogram only. However, it can honor the local conditioning data and integrate secondary information faster and easier.

Because of the sparse sampling of well data, it is important to integrate information from seismic data that delivers better areal coverage (Fournier, 1995; Haas and Dubrule, 1994; Tjolsen and others, 1995; Xu, 1995). However, seismic data always provide information on a larger scale than the well log data, and are considered equivalent to 2D data when building 3D lithofacies models. Integration of data defined on such different scales is a difficult challenge. Several algorithms have been proposed to integrate the seismic data. One proposal is to repeat the 2D seismic attribute profile along each vertical slice, thus creating artificially dense 3D seismic data. They are then used as prior means or as covariates in a Markov-Bayes algorithm (Zhu and Journel, 1993). The other proposal is to integrate the 2D seismic data interpreted as a block average value and honor these data using simulated annealing (Deutsch, Srinivasan, and Mo, 1996) or block cokriging (Behrens, Macleod, and Tran, 1996). Simulated-annealing algorithms require delicate tuning of the annealing schedule parameters to reach convergence and may be cpu-intensive.

In this paper, we focus on three algorithms based on sequential indicator simulation for integrating seismic information: (1) integrating seismic data as a prior mean; (2) integrating seismic data as a collocated block value; and (3) integrating seismic data with the Markov-Bayes algorithm. All these algorithms are applied to a synthetic data set generated from a real clastic reservoir. The results are compared with regard to how the correlation between seismic data and well log data is honored. The pros and cons of these different algorithms in different situations are discussed.

RECALL OF CELL-BASED SEQUENTIAL INDICATOR SIMULATION ALGORITHMS (sisim)

The cell-based indicator simulation algorithm is based on sequential simulation. At each node of the simulation grid, the local lithofacies probability distribution function conditional to both original data and previously simulated values is determined, followed by drawing the lithofacies type from that local distribution. The new drawn lithofacies value is then used as conditioning data for the nodes to be simulated later, hence the name "sequential indicator simulation."

Assuming there are altogether K lithofacies, each original lithofacies datum is recoded as a vector of binary indicator $[i(\mathbf{u}_\alpha; k), k = 1, \ldots, K]$ with

$$i(\mathbf{u}_\alpha; k) = \begin{cases} 1 & \text{if } \mathbf{u}_\alpha \in \text{lithofacies } k \\ 0 & \text{otherwise} \end{cases} \tag{1}$$

The conditional probability of occurence of lithofacies k at any unsampled location $\mathbf{u}$ is estimated by indicator kriging as (Goovaerts, 1997, p. 293)

$$\text{Prob}\{Z(\mathbf{u}) = k \mid (n)\} = E\{I(\mathbf{u}; k) \mid (n)\} = i^*(\mathbf{u}; k), \quad k = 1, \ldots, K$$

with

$$i^*(\mathbf{u}; k) - p_k = \sum_{\alpha=1}^{n} \lambda_\alpha(\mathbf{u}; k)[i(\mathbf{u}_\alpha; k) - p_k] \tag{2}$$

where $p_k = E\{I(\mathbf{u}; k)\}$ is the global proportion of lithofacies k; the notation (n) means "conditioning to the n neighborhood data available": these include both original data and previously simulated values. λ_α represent the weights determined by solving the kriging system. Note that the best estimation of $i^*(\mathbf{u}; k)$ could be achieved by cokriging involving all the indicator data $i^*(\mathbf{u}_\alpha; l), l = 1, \ldots, K$. That requires inference of all the auto- and cross-indicator covariance models, which is not applicable in reality.

The indicator kriging process is repeated for the K lithofacies; the resulting conditional probabilities $i^*(\mathbf{u}; k)$ are then assembled into a cumulative conditional distribution function, or ccdf:

$$\prod(\mathbf{u}; k) = \sum_{k'=1}^{k} i^*(\mathbf{u}; k') \in [0, 1]$$

The simulated lithofacies type at $\mathbf{u}$ is obtained by a Monte Carlo sampling from that local ccdf. The ordering of the lithofacies while assembling the ccdf can be arbitrary since it does not affect the facies type from Monte Carlo sampling.

Note that the set of conditional probabilities $i^*(\mathbf{u})$ may not verify the order relation condition, that is, $i^*(\mathbf{u}) \in [0, 1]$ and $\prod(\mathbf{u}; K) = \sum_{k'=1}^{K} i^*(\mathbf{u}; k') = 1$. Therefore, correction for order relations needs to be made prior to the Monte Carlo sampling (Deutsch and Journel, 1998). This might have an impact on the reproduction of indicator variogram models, depending on the correction magnitude (Deutsch and Journel, 1998).

The major advantage of sequential indicator simulation, which is based on indicator kriging, is that it can account for soft data in a fast and robust way while generating the conditional distributions, provided that the soft data can be coded as a prior local probability value.

Integrating Seismic Data as Prior Local Mean

With seismic data providing information about the local prior probability $p_k(\mathbf{u})$ of facies k prevailing at location $\mathbf{u}$, the simple indicator kriging expression (2) can be written as follows:

$$i^*(\mathbf{u}; k) - p_k(\mathbf{u}) = \sum_{\alpha=1}^{n} \lambda_\alpha(\mathbf{u}; k)[i(\mathbf{u}_\alpha; k) - p_k(\mathbf{u})] \tag{3}$$

Note that expression (3) requires knowledge of the prior local mean $p_k(\mathbf{u})$ at every grid location $\mathbf{u}$, that is, at the resolution of the 3D modeling grid. But, seismic data typically do not have the same vertical resolution as that of the geological model. They usually represent some averaged proportions of each lithofacies along vertical lines, hence are considered as 2D data. The assumption that a seismic measurement provides the same information at different vertical levels of the 3D modeling grid amounts to duplicating the actual 2D seismic value along the vertical lines to generate artificial 3D data, that is, $p_k(\mathbf{u}) = p_k(\mathbf{x})$, where $\mathbf{u} = (\mathbf{x}, z)$ (Goovaerts, 1997, p. 190; Gorell, 1995). This duplication could lead to some vertical banding in the 3D realization if the vertical range is relative short and the kriging weight on the prior mean in high.

Note that in the simple kriging estimate of Equation (3), we assumed that the prior local mean is stationary within the search neighborhood although it will change with the estimation location $\mathbf{u}$. Therefore, Equation (3) can also be written as

$$i^*(\mathbf{u}; k) = \sum_{\alpha=1}^{n} \lambda_\alpha(\mathbf{u}; k) i(\mathbf{u}_\alpha; k) + \lambda_0 p_k(\mathbf{u}) \tag{4}$$

with $\lambda_0 = 1 - \sum_{\alpha=1}^{n} \lambda_\alpha$ being the weight applied on the prior local mean $p_k(\mathbf{u})$ provided by seismic data. The corresponding simple kriging system determining

the weights $\lambda_\alpha(\mathbf{u};k)$ is

$$\sum_{\beta=1}^{n}\lambda_\beta C_I(\mathbf{u}_\beta-\mathbf{u}_\alpha;k)=C_I(\mathbf{u}-\mathbf{u}_\alpha;k),\quad \alpha=1,\ldots,n \tag{5}$$

where $C_I(\mathbf{u}_\beta-\mathbf{u}_\alpha;k)$ is calculated from the indicator variogram model for lithofacies k.

The weight $\lambda_0=1-\sum_{\alpha=1}^{n}\lambda_\alpha$ applied on the local mean depends on all the λ_α, which are dependent only on the spatial structure, that is, the indicator variogram model of the lithofacies. As the continuity range of the indicator variogram model increases, the weights λ_α increases. The weight, λ_0, applied on seismic data decreases as a consequence. The influence of seismic data usually diminishes as more previously simulated values in the search neighborhood are used as conditioning data. This can be seen in the later section of case study. For this algorithm, there is no other free parameter to impose a higher weight on seismic data.

Integrating Seismic Data as Collocated Block Value

Seismic data have limited vertical resolution, and so only provide estimates of the 2D areal distribution of vertical lithofacies proportions. In the kriging expression (2), the processed seismic data of lithofacies proportion $s(\mathbf{x};k)$ at the horizontal location $\mathbf{x}=(x,y)$ of the 3D grid location $\mathbf{u}=(\mathbf{x};z)$ is added as a "block average" value (Abrahamsen and others, 1996; Behrens, Macleod, and Tran, 1996; Haas and Natinger, 1996; Journel 1999; Journel and Huijbregts, 1978, p. 305), where z represents the vertical coordinate of the location $\mathbf{u}$. The 2D seismic value $s(\mathbf{x};k)$ is common to all lithofacies indicator variables $i(\mathbf{u};k)$ along the vertical line at $\mathbf{x}$ but its correlation with $i(\mathbf{u};k)$ is specific to the lithofacies k and the coordinate z of $\mathbf{u}=(\mathbf{x};z)$. Its relation to the vertical average of the indicator variable $i(\mathbf{u};k)$ is approximated as

$$s(\mathbf{x};k)\approx\frac{1}{n_z}\sum_{1}^{n_z}i(\mathbf{x},z;k) \tag{6}$$

where n_z is the number of vertical cells penetrated by vertical or horizontal wells. Although this relation is not directly supported by physics for the original data from seismic survey, geophysicists can process the seismic volume of amplitude and derive a map informing areal lithofacies proportions, based on calibration between seismic data and lithofacies proportion at well locations (Yao and Chopra, 2000).

The kriging estimate is then written as

$$i^*(\mathbf{u};k) - p_k = \sum_{\alpha=1}^{n} \lambda_\alpha(\mathbf{u};k)[i(\mathbf{u}_\alpha;k) - p_k] + \lambda_0[s(\mathbf{x};k) - p_k] \tag{7}$$

The seismic data $s(\mathbf{x};k)$ are introduced through an additional term in the kriging expression. Because of the linearity of expression (6), the correlation between $s(\mathbf{x};k)$ and any value $i(\mathbf{u};k)$ is simply

$$\bar{C}_I(\mathbf{u}_\alpha, \mathbf{x};k) = \mathrm{Cov}\{I(\mathbf{u}_\alpha;k), S(\mathbf{x};k)\} = \frac{1}{n_z}\sum_{z=1}^{n_z} C_I\{I(\mathbf{x}, z;k), S(\mathbf{x};k)\}$$

where n_z is the number of vertical cells penetrated by vertical or horizontal wells at horizontal location $\mathbf{x}$.

The corresponding kriging system derived from (7) is

$$\begin{cases} \sum_{\beta=1}^{n} \lambda_\beta C_I(\mathbf{u}_\beta - \mathbf{u}_\alpha;k) + \lambda_0 \bar{C}_I(\mathbf{u}_\alpha, \mathbf{x};k) = C_I(\mathbf{u} - \mathbf{u}_\alpha;k), \quad \alpha = 1, \ldots, n \\ \sum_{\beta=1}^{n} \lambda_\beta \bar{C}_I(\mathbf{u}_\beta, \mathbf{x};k) + \lambda_0 \ \mathrm{Var}\{S(\mathbf{x};k)\} = \bar{C}_I(\mathbf{u}, \mathbf{x};k) \end{cases} \tag{8}$$

where

$$\mathrm{Var}\{S(\mathbf{x};k)\} = \frac{1}{n_z^2}\sum_{z=1}^{n_z}\sum_{z'=1}^{n_z} C_I\{I(\mathbf{x}, z;k), I(\mathbf{x}, z';k)\}$$

This calculated theoretical seismic data variance $\mathrm{Var}\{S(\mathbf{x};k)\}$ needs to be increased by the relevant amount of noise or obtained from the experimental variance.

If all the estimated nodes $\mathbf{u} = (\mathbf{x}, z)$ at the same $\mathbf{x}$ but different z locations utilize the same data configuration, then the vertical average of the resulting 3D estimated values $i^*(\mathbf{u};k)$ identify the 2D conditioning seismic data, that is, $\frac{1}{n_z}\sum_{z=1}^{n_z} i^*(\mathbf{x}, z;k) = s(\mathbf{x};k), \ \forall \mathbf{x}$. The proof for this exactitude property is provided by Journel (1999). However, in a sequential simulation paradigm where previously simulated values are added as conditioning data for the nodes to be simulated later, it is difficult to keep the same data configuration for all nodes along the same vertical line. As simulation proceeds, more previously simulated nodes close to the current node are to be used as conditioning data. If the vertical range of the variogram model is relatively short compared with the horizontal range the weight λ_0 applied to the block value $s(\mathbf{x};k)$ may be small, resulting in an estimated average value $\frac{1}{n_z}\sum_{z=1}^{n_z} i^*(\mathbf{x}, z;k)$ that is not very well correlated with the input seismic data $s(\mathbf{x};k)$. Therefore, the correlation between the 2D proportion

values calculated from the 3D models and the input seismic proportion map also depends on the range of the indicator variogram model, as in the algorithm integrating seismic data as local mean.

Integrating Seismic Data With the Markov-Bayes Algorithm

Similar to sequential indicator simulation (sisim) with prior local mean, sisin with the Markov-Bayes algorithm (Zhu and Journel, 1993) also requires that seismic data have the same resolution as the geological model. Hence, the 2D seismic proportions need to be duplicated vertically to match the small scale of 3D geological model. However, contrary to sisim with local mean, the local prior probability data $y(\mathbf{u};k)$ is used as secondary data in an indicator cokriging system (Deutsch and Journel, 1998), that is,

$$i^*(\mathbf{u};k) - p_k = \sum_{\alpha=1}^{n} \lambda_\alpha(\mathbf{u};k)[i(\mathbf{u}_\alpha;k) - p_k] + \nu(\mathbf{u};k)[y(\mathbf{u};k) - p_k] \qquad (9)$$

with $\nu(\mathbf{u};k)$ being the weight applied on the seismic data.

The corresponding kriging system is

$$\begin{cases} \sum_{\alpha=1}^{n} \lambda_\alpha(\mathbf{u};k) C_I(\mathbf{u}_{\alpha_1} - \mathbf{u}_\alpha;k) + \nu(\mathbf{u};k) C_{IY}(\mathbf{u}_{\alpha_1} - \mathbf{u};k) = C_I(\mathbf{u}_{\alpha_1} - \mathbf{u};k) \\ \qquad\qquad\qquad\qquad\qquad\qquad\qquad\qquad\qquad\qquad \alpha_1 = 1, \ldots, n(\mathbf{u}) \\ \sum_{\alpha=1}^{n} \lambda_\alpha(\mathbf{u};k) C_{IY}(\mathbf{u}_{\beta_1} - \mathbf{u}_\alpha;k) + \nu(\mathbf{u};k) C_Y(0;k) = C_{YI}(0;k) \end{cases} \qquad (10)$$

This cokriging system calls for one autocovariance model of $C_I(\mathbf{h};k)$, one cross-covariance model of $C_{IY}(\mathbf{u};k)$, and the autocovariance value of $C_Y(0;k)$. The modeling can be alleviated by a Markov-type hypothesis, leading to the following relation (Zhu and Journel, 1993):

$$C_Y(\mathbf{h};k) \begin{cases} = B(k) C_I(\mathbf{h};k) & \mathbf{h} = 0 \\ = B^2(k) C_I(\mathbf{h};k) & \mathbf{h} > 0 \end{cases} \qquad (11)$$

and

$$C_{IY}(\mathbf{h};k) = B(k) C_I(\mathbf{h};k) \qquad (12)$$

where $B(k)$ is defined as the difference between the two conditional expectations:

$$B(k) = m^{(1)}(k) - m^{(0)}(k) \in [-1, 1], \quad k = 1, \ldots, K$$

with

$$m^{(1)}(k) = E\{Y(\mathbf{u};k) \mid I(\mathbf{u};k) = 1\} \in [0,1]$$
$$m^{(0)}(k) = E\{Y(\mathbf{u};k) \mid I(\mathbf{u};k) = 0\} \in [0,1]$$

The parameter $B(k)$ can be obtained by the calibration between collocated hard indicator data and soft probability data. It measures how well the soft y data separate the two cases: $i = 1$ and $i = 0$, that is, the accuracy of the soft data. If $B(k) = 1$, then $C_Y(\mathbf{h};k) = C_{IY}(\mathbf{h};k) = C_I(\mathbf{h};k)$, there is no updating of the soft data $y(\mathbf{u};k)$, hence $i^*(\mathbf{u};k) = y(\mathbf{u};k)$.

If $B(k) = 0$, then $C_{IY}(\mathbf{h};k) = 0$, and the soft data will receive 0 weight.

As opposed to sisim with local mean or sisim with block cokriging, one flexibility gained with the Markov-Bayes algorithm is that the weight on the soft data $\nu(\mathbf{u};k)$ is dependent both on the indicator variogram model and the calibration coefficient $B(k)$. To increase the contribution of seismic data, which is desired in some cases, the $B(k)$ can be adjusted to a high value to achieve higher weight on the secondary seismic data. In the extreme case, when $B(k) = 1$, the prior proportion from seismic data is not updated, so the final lithofacies model is drawn from the seismic-derived proportion. The vertical averaged lithofacies proportions from the 3D lithofacies model honor the seismic proportions. This can be seen in the following case study.

CASE STUDY AND COMPARISON

For this case study, a synthetic data set generated from a North Sea clastic reservoir is used (Journel and others, 1998). The area of the modeling field is 5050×6550 ft^2.

The good-quality sand (pay lithofacies) in this reservoir is deposited in channels. Based on 20 wells, the volume proportion of channel sand relative to the total model is 33%. Mudstone and other lithofacies constitute the remaining model volume 67%. The average gross thickness of the reservoir is 20 ft, with lithofacies description in cores available at a 1 ft interval. Thus, the modeling grid vertical resolution was set at 1 ft. This grid includes 101×131 horizontal nodes with a 50 ft spacing. The available information includes the 20 wells with lithofacies indicator data and synthetic seismic data. The synthetic seismic data were generated as follows: a 3D lithofacies model from the study given in Journel and others (1998) is taken to calculate the average lithofacies proportion along the vertical lines. The resulting 2D sand proportion map was then smoothed through moving average. Therefore, the seismic data in this case inform the lithofacies proportions areally. This study assumed they are very accurate and need to be honored as well as possible.

Figure 1 shows maps of sand proportion from seismic data (Fig. 1(A)) and the well locations (Fig. 1(B)). The scatterplot between the prior seismic-derived sand

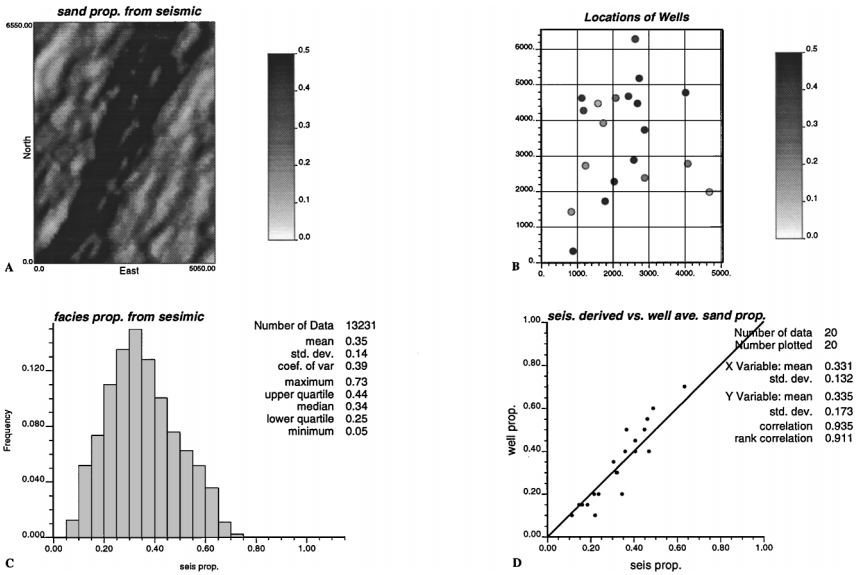

Figure 1. Seismic map of lithofacies proportions and the 20 well locations. (A) Sand proportion map from seismic data; (B) location map of 20 wells; (C) histogram of sand proportions from seismic; (D) scatterplot between seismic derived proportion and well averaged sand proportion.

proportion and the collocated 20-well proportion data indicates a linear correlation at 0.935 (Fig. 1(D)), although the standard deviation of the sand proportion in seismic data is smaller compared to that from well data (0.13 vs. 0.17, Fig. 1(C)) due to the smoothing of seismic data. This correlation coefficient is much higher than in real situations, which is expected to be reproduced by the different methods.

Figure 2 shows the experimental vertical indicator variograms of channel sand calculated from the lithofacies indicator data along the wells, indicating a vertical

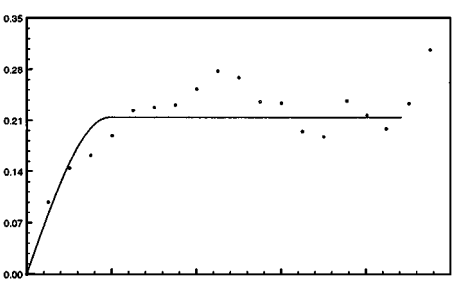

Figure 2. Experimental indicator variogram of sand lithofacies in the vertical direction, calculated from the 20 wells.

range of about 4 ft. Due to the sparsity of lateral data (only 20 well locations), the horizontal ranges were obtained from geological interpretation, with 700 ft range in N60°W direction and 7000 ft range in N30°E direction. The semivariogram model is

$$\gamma(\mathbf{h}) = 0.22Sph\left(\sqrt{\left(\frac{h_1}{7000}\right)^2 + \left(\frac{h_2}{700}\right)^2 + \left(\frac{h_z}{4}\right)^2}\right) \tag{13}$$

The study objectives are as follow:

- integrate the seismic information using the three different algorithms;
- determine how much weight is applied to the prior seismic information from solving the kriging system;
- check how well the correlation between the vertically averaged lithofacies proportion from 3D lithofacies model and prior seismic derived proportion is reproduced;
- check sensitivity of the contribution of seismic information with regard to the range of the variogram model.

Using the given semivariogram model in (13), different realizations can be generated from the previously described three algorithms. For the Markov-Bayes algorithm, the calibration between the 20 wells and collocated seismic data provides coefficient $B = 0.265$ for both sand and shale lithofacies.

Figure 3 shows the weights applied on the seismic proportions versus the number of previously simulated values for different algorithms. Typically, as the simulation proceeds, in the search neighborhood, most of the conditioning data are previously simulated values that are very close to the node being simulated. Given the long range spatial structure of channels, the weights given to these neighboring data are very high, leaving only a small portion of weight to the

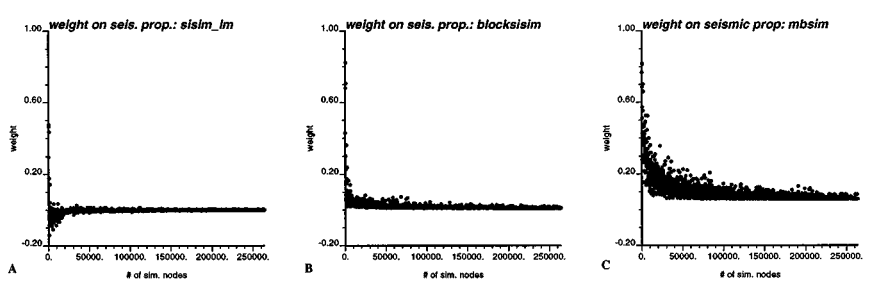

Figure 3. Kriging weight applied to the seismic proportion data versus the number of previously simulated nodes: (A) sisim with seismic data as local mean; (B) sisim with seismic data as block value; (C) sisim with seismic data integrated through Markov-Bayes algorithm.

seismic data. For sisim with local mean (Fig. 3(A)), the weight given to seismic data is close to 0, with most of them even below 0. Hence, the seismic data do not contribute much to modeling, given the positive correlation between seismic data and well proportions. Although sisim with local mean is easy to implement, it is not widely applied due to this disadvantage, especially at an early appraisal stage of the reservoir when the seismic data need to be fully accounted for. For sisim with seismic data integrated as block values, the weights applied on seismic data decrease systematically as the sequential simulation process advances. Most of the weights are near 0. For the Markov-Bayes algorithm, the weights on the seismic data as covariates are significantly higher than those from the other two algorithms. Moreover, all the weights are greater than 0 even when the number of previously simulated values is large. The comparison of these weights shows that the seismic proportion contributes most in the Markov-Bayes algorithm, whereas it contributes least in the sisim with local mean algorithm. In a recent paper, Yao and Chopra (2000) show that for sisim with seismic block value, the contribution of seismic data increases as the number of previously simulated values retained for kriging decreases.

Figure 4 shows the scatterplot between the sand proportion calculated from the vertical average of the simulated 3D lithofacies model and the input seismic proportions. Again, the Markov-Bayes algorithm provides the largest correlation coefficient (0.78) while sisim with local mean gives the smallest correlation coefficient (0.43). However, none of them meet our objective to reproduce the scatterplot from calibration data shown in Figure 1 (0.935).

For visualization purposes, the sand proportions from the vertical averages of these 3D models are shown in Figure 5, to be compared with the input seismic proportion map of Figure 1(A). Again, the proportion map using sisim with local mean does not honor well the high- or low-sand proportion patches observed in the seismic proportion map. Note also that the curvilinear structure or crisp shape of channels observed in Figure 1(A) is not reproduced by the sequential indicator simulation algorithms.

To study the sensitivity of the contribution of seismic data relative to the range of the spatial structure of lithofacies, we artificially decreased the horizontal range of the variogram model in (13) to 1000 ft, 100 ft in the horizontal major directions, and kept the vertical range at 4 ft. By decreasing the range, the kriging weights on the previously simulated values are expected to decrease, so the weight on the seismic data is expected to increase in all three algorithms. Figure 6 shows the plot of weights on seismic data versus the number of previously simulated values. Compared to Figure 3, it indeed shows higher weights on the seismic data, although more scattered. Similarly, Figure 7 shows the scatterplot between the vertically averaged sand proportion from the 3D model and the seismic derived proportion. The correlation coefficients have been increased in all cases compared to Figure 4. Figure 8 provides a visual comparison to the seismic proportion map in

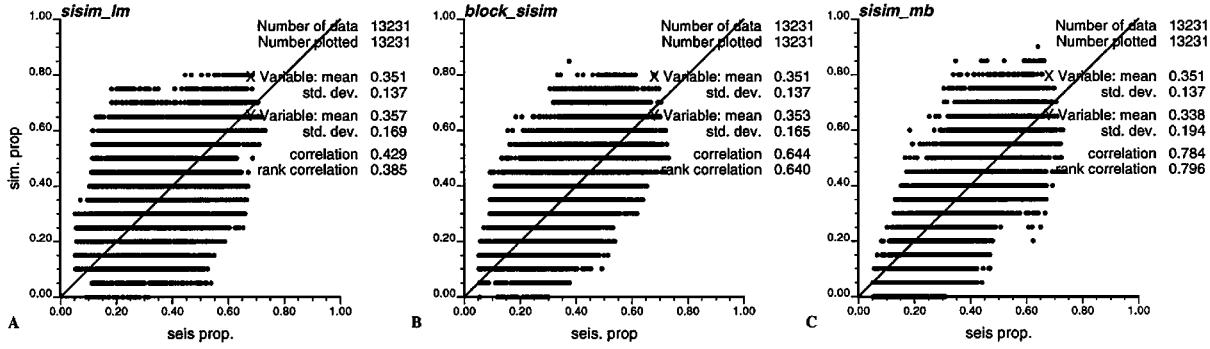

Figure 4. Scatterplot of the lithofacies proportions calculated from the 3D lithofacies model versus the input seismic proportion map: (A) sisim with seismic data as local mean; (B) sisim with seismic data as block value; (C) sisim with seismic data integrated in Markov-Bayes algorithm.

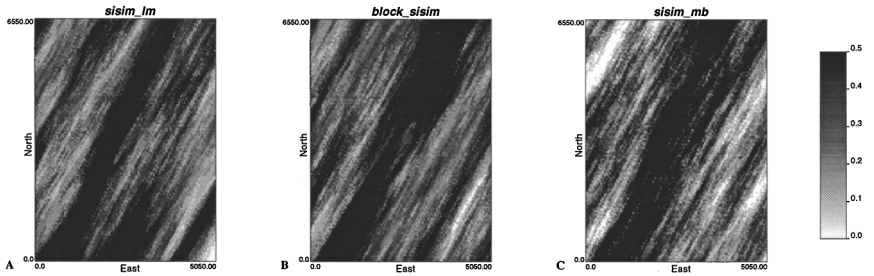

Figure 5. Facies proportion maps calculated from the 3D lithofacies models generated through different algorithms: (A) sisim with seismic data as local mean; (B) sisim with seismic data as block value; (C) sisim with seismic data integrated in Markov-Bayes algorithm.

Figure 1. This illustrates that as the facies indicator variogram range decreases, the seismic proportion contributes more to the modeling of lithofacies. However, in real practice, it is not appropriate to decrease the range arbitrarily. In fluvial reservoirs, the channel sand usually has greater spatial continuity in the paleocurrent direction, which should be honored in the model. Simultaneously, useful information from seismic needs to be fully incorporated due to the sparse sampling from well data. Neither sisim with seismic data as local mean nor sisim with seismic data in block cokriging can take full account of the seismic information without an artificial decrease of the variogram range.

The only algorithm that has the flexibility of increasing the seismic contribution without decreasing the variogram range is Markov-Bayes algorithm, that is, by tuning the B coefficient. Figure 9 shows the result using $B = 0.6$ while keeping the range of 7000, 700, and 4 ft. The weights are higher and the correlation with the seismic derived proportion is increased as well, compared to Figures 3(C) and 4(C).

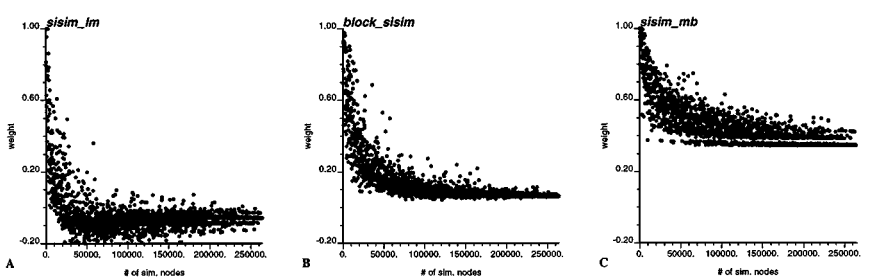

Figure 6. Similar to Figure 3, except that the horizontal variogram ranges are 10 times less. (A) Sisim with seismic data as local mean; (B) sisim with seismic data as block value; (C) sisim with seismic data integrated in Markov-Bayes algorithm.

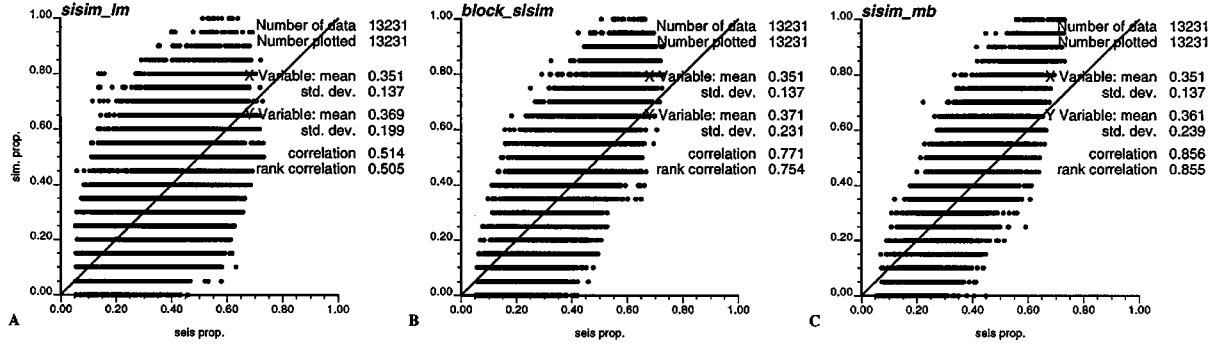

Figure 7. Similar to Figure 4, except that the horizontal variogram ranges are 10 times less. (A) Sisim with seismic data as local mean; (B) sisim with seismic data as block value; (C) sisim with seismic data integrated in Markov-Bayes algorithm.

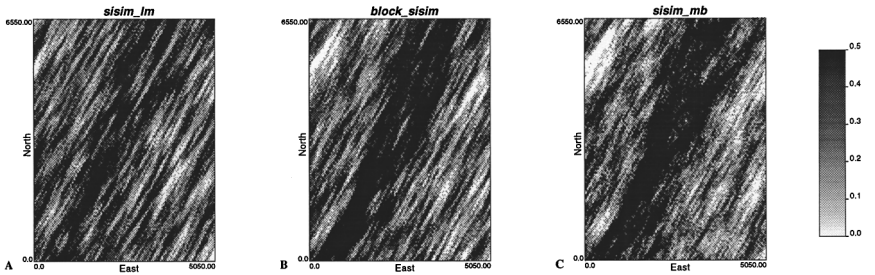

Figure 8. Similar to Figure 5, except that the horizontal variogram ranges are 10 times less. (A) Sisim with seismic data as local mean; (B) sisim with seismic data as block value; (C) sisim with seismic data integrated in Makov-Bayes algorithm.

CONCLUSIONS AND DISCUSSION

This paper explores the integration of seismic data for building 3D geological models of lithofacies. The sequential indicator simulation algorithm is modified to integrate seismic lithofacies proportions using three different algorithms: as local mean, as collocated block value, and as covariate with the Markov-Bayes algorithm. The contribution of seismic information was compared for each of the three algorithms, and the sensitivity of the contribution relative to the spatial continuity range of lithofacies was studied.

For lithofacies distributions having short range of continuity, sisim with local mean can account for the seismic information reasonably well. Also, the advantage of sisim with local mean is the easy implementation and short cpu time in solving for the kriging weights, but there may be some vertical banding in some cases. For lithofacies distributions having long range of continuity, the Markov-Bayes algorithm can take full account of the seismic information through a tuning of the

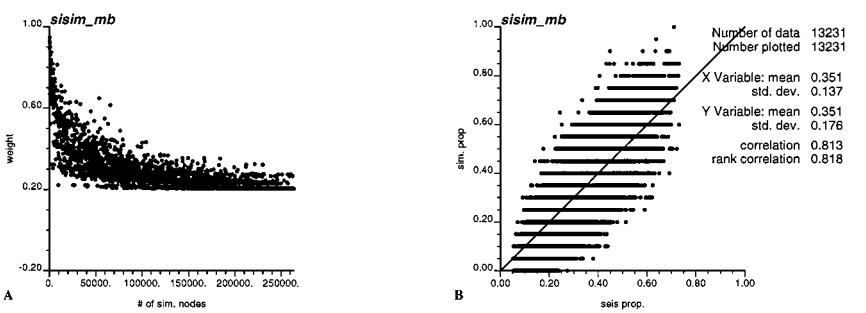

Figure 9. Similar to Figure 3(C) and Figure 4(C), except that the *B* value is 0.60. (A) Kriging weight applied to the seismic proportion data versus the number of simulated values; (B) scatterplot of sand proportions calculated from the 3D facies model versus the input seismic proportion map.

calibration coefficient B values. For lithofacies distributions with long continuity range in the vertical direction, sisim with collocated block value will have a higher contribution from the seismic data, but at the cost of greater cpu time due to the calculation of block covariances and one additional equation in the kriging system.

All of these algorithms can be extended to simulate a continuous variable, such as porosity. For example, the seismic data may provide vertically averaged porosity values over the whole field. The same observation and conclusions drawn in this case study are expected to hold for such continuous variables.

REFERENCES

Abrahamsen, P., Hektoen, A. L., Holden L., and Munthe, K. L., 1996, Seismic impedance and porosity: Support effect, *in* Baffi, S., ed., Geostatistics Wollongong 96, Vol. 1: Kluwer, Dordrecht, p. 489–500.

Behrens, R. A., Macleod, M. K., and Tran, T. T., 1996, Incorporating seismic attribute maps in 3D reservoir models: Paper presented at the annual SPE meeting, Denver, CO, SPE paper no. 36499.

Deutsch, C., and Journel, A., 1998, GSLIB: Geostatistical software library and user's guide, 2nd edn.: Oxford University Press, New York, 368 p.

Deutsch, C. V., Srinivasan, S., and Mo, Y., 1996, Geostatistical reservoir modeling accounting for precision and scale of seismic data: Paper presented at the SPE annual meeting, Denver, CO, SPE paper no. 36497.

Deutsch, C., and Wang, L., 1996, Hierarchical object-based stochastic modeling of fluvial reservoirs: Math. Geol., v. 28, no. 7, p. 857–880.

Fournier, F., 1995, Integration of 3D seismic data in reservoir stochastic simulations: A case study: Paper presented at the annual SPE meeting, Dallas, TX, SPE paper no. 30564.

Georgsen, F., and Omre, H., 1993, Combining fiber processes and Gaussian random functions for modeling fluvial reservoirs, *in* Soares, A., ed., Geostatistics-Troia: Kluwer, Dordrecht, p. 425–440.

Goovaerts, P., 1997, Geostatistics for natural resources evaluation: Oxford University Press, New York, 483 p.

Gorell, S. B., 1995, Creating 3D reservoir models using areal geostatistical techniques combined with vertical well data: Paper presented at the western regional meeting, Bakersfield, CA, SPE paper no. 29670, p. 967–974.

Haas, A., and Dubrule, O., 1994, Geostatistical inversion: A sequential method of stochastic reservoir modeling constrained by seismic data: First Break, v. 12, no. 11, p. 561–569.

Haas, A., and Natinger, B., 1996, Stochastic reservoir modeling constrained by well test permeability, *in* Baffi, S., ed., Geostatistics Wollongong 96, Vol. 1: Kluwer, Dordrecht, p. 501–511.

Haldorsen, H. H., and Damsleth, R., 1990, Stochastic modeling: J. Pet. Technol., v. 42, no. 4, p. 404–412.

Journel, A., 1999, Conditioning geostatistical operations to non-linear volume averages: Math. Geol., v. 31, no. 8, p. 931–954.

Journel, A., and Alabert, F., 1989, Non-Gaussian data expansion in the earth science: Terra Nova, v. 1, p. 123–134.

Journel, A., and Alabert, F., 1990, New method for reservoir mapping: J. Pet. Technol., v. 42, no. 2, p. 212–218.

Journel, A., Gundeso, R., Gringarten, E., and Yao, T., 1998, Stochastic modeling of a fluvial reservoir: A comparative review of algorithms: J. Pet. Sci. Eng., v. 21, p. 95–121.

Journel, A., and Huijbregts, Ch., 1978, Mining geostatistics: Academic Press, London, 600 p.

Omre, H., Solna, K., and Tjelmeland, H., 1990, Calcite cementation description and production consequences: Paper presented at the 1990 SPE annual technical conference and exhibition, New Orleans, OK, SPE paper no. 20607.

Stoyan, D., Kendall, W., and Mecke, J., 1987, Stochastic geometry and its applications: Wiley, New York, 436 p.

Tjolsen, C. B., Johnsen, G., Halvorsen, G., Rtseth, A., and Damsleth, E., 1995, Seismic data can improve the stochastic lithofacies modeling significantly: Paper presented at the SPE annual meeting, Dallas, TX, SPE paper no. 30567.

Xu, W., 1995, Stochastic modeling of reservoir lithofacies and petrophysical properties: Unpublished doctoral dissertation, Stanford University, 214 p.

Yao, T., and Chopra, A., 2000, Integration of 2D seismic data into 3D lithofacies modeling: J. Pet. Sci. Eng., v. 27, p. 69–84.

Zhu, H., and Journel, A., 1993, Formatting and integrating soft data: Stochastic imaging via the Markov-Bayes algorithm, *in* Soares, A., ed., Geostatistics-Troia: Kluwer, Dordrecht, p. 1–12.